Nanoscale

PAPER

View Article Online
View Journal | View Issue

Cite this: *Nanoscale*, 2020, **12**, 12917

The enzyme-induced formation of iron hybrid nanostructures with different morphologies†

Rocio Benavente,[a] David Lopez-Tejedor,[a] Maria del Puerto Morales,[b] Carlos Perez-Rizquez[a] and Jose M. Palomo *[a]

Received 21st April 2020,
Accepted 27th May 2020

DOI: 10.1039/d0nr03142a

rsc.li/nanoscale

A new synthesis method for tailor-made iron-hybrid nanoparticles has been carried out for the first time using enzymes, which directly induce the formation of inorganic iron species. The role of the protein was critical for the formation and morphology of the iron nanostructures and, depending on the enzyme, by simple mixing with ammonium iron(II) sulfate at room temperature and under air, it was possible to obtain, for the first time, well stabilized superparamagnetic iron and iron oxide nanorods, nanosheets and nanorings or even completely amorphous non-magnetic iron structures in the protein network. These iron nanostructure-enzyme hybrids showed excellent results as heterogeneous catalysts in organic chemistry (chemoselective hydrogenation and C–C bonding formation) and environmental remediation processes.

Introduction

Iron nanoparticles have gained important relevance in different areas over the last few years, with special focus on biomedical applications.[1–4]

Magnetic resonance imaging (MRI) contrast agents and drug delivery are two of the areas of greatest application of these nanoparticles, precisely because of the properties of these iron nanoparticles; they offer high magnetic saturation, stability, biocompatibility, and interactive functions at the surface.[5,6]

Recently, considering the importance of sustainability, iron compounds have exhibited tremendous growth in their application as catalysts.[7–9]

Although the efficiency of iron cannot be compared to such metals as Pd or Au in many organic chemical reactions, the application of nanostructures has advantages in order to obtain higher catalytic efficiency, based on their high surface-to-volume ratio compared to bulk materials.[10–12] Also the magnetism of iron nanoparticles gives them an advantage since they are easily recovered from reaction solutions by external magnetic fields, reducing energy consumption and catalyst loss, and saving time in catalyst recovery.[13]

The main challenge in this case is obtaining small size nanoparticles due to their tendency to aggregate, not only because of their small size but also due to the presence of magnetic interactions. The control of the size is therefore a critical issue for the production of excellent catalysts.[14]

The successful development of synthetic strategies[15–17] has made these iron nanostructures tremendously interesting catalysts applied in different areas. One of these areas is synthetic cross-coupling (C–C, C–O) reactions, recently successfully described by using supported-iron oxide nanoparticles, alone or combined with other metals.[18,19]

In this context, new technologies allowing the synthesis of iron nanostructures under mild conditions using simple processes, without needing additional equipment, would have a remarkable impact.

In a previous communication, we reported the use of a greener synthetic methodology to synthesize iron carbonate nanorods into a nanohybrid structure.[20] For that, a hydrolase was used as an inductor controlling the synthesis, iron species and final morphology, creating well-dispersed iron nanorods in the biological matrix, avoiding any aggregation problems. However, stabilization of the iron species is not an easy task, because of the extremely fast oxidative process.

Therefore, here we have extended the application of enzymes to induce the formation of iron nanoparticles in aqueous media and at room temperature, evaluating the experimental conditions to completely avoid oxidation and control the species. The effect of using different enzymes from different sources and of different molecular weight, with monomeric or multimeric structures on the iron species, and different nanoparticle sizes and magnetic properties has been studied. These iron nanoparticles-enzyme nanobiohybrids are heterogeneous materials and their catalytic capacity in different organic chemical reactions and environmental processes was evaluated.

[a]*Department of Biocatalysis, Institute of Catalysis (ICP-CSIC), Marie Curie 2, 28049 Madrid, Spain. E-mail: josempalomo@icp.csic.es; Fax: (+34)-91-5854760*
[b]*Department of Energy, Environment and Health, Institute of Material Science of Madrid (ICMM-CSIC), Sor Juana Ines de la Cruz 3, 28049 Madrid, Spain*

†Electronic supplementary information (ESI) available. See DOI: 10.1039/d0nr03142a

Results and discussion

Synthesis and characterization of iron nanoparticles-enzyme hybrids

Firstly, liquid commercial hydrolase (*Candida antarctica B* lipase (CALB)) was dissolved in buffer solution (pH from 5 to 10) and different concentrations of solid $(NH_4)_2Fe(SO)_2$ (Mohr's salt) were added. Considering our previous results in the formation of palladium nanoparticles induced by this hydrolase,[21] a cloudy solution is indicative of the formation of a hybrid between the enzyme and metals for the final generation of nanoparticles. Solutions with pH lower than 6 (isoelectric point of the enzyme) and with an amount of iron salt lower than 10 mg mL^{-1} did not form any cloudy solution. Thus, the best initial conditions were obtained by using solutions containing bicarbonate buffer at pH 10 and 10 mg ml^{-1} of iron salt. During the initial step of the incubation (around 30 min), the pH of the solution was evaluated and had decreased to pH 8, and then remained unaltered during the entire incubation time. After incubation with magnetic stirring at room temperature for 16 hours, a dark green solid was obtained (Fig. S1†), which was washed several times with distilled water, centrifuged and finally lyophilized overnight.

X-ray diffraction (XRD) analysis revealed that the enzyme induced the formation of iron(II) carbonate (siderite, $FeCO_3$) (matched well with JCPDS no. 29-696) as the main iron species, containing a very small amount of other oxidative species (hematite) (Fig. 1). Indeed, controlling the stirring speed to 380 rpm was a key parameter to obtain this iron species. Experiments performed at higher or even uncontrolled stirring speeds led to the formation of hematite (orange solid), as well as the use of other methods such as roller stirring (Fig. S1†). To remove this iron oxide species, an additional reduction step was introduced after the incubation time.

At this point, we added sodium borohydride and evaluated the effect of different reduction times. XRD analysis showed that the peak at around 36° was almost completely eliminated after a 15 min reduction (Fig. 1) and XPS confirmed that iron carbonate was the only species (Fig. S2†). XRD also showed that this peak started to grow again if the reduction time was prolonged due to the rapid oxidation of iron (Fig. 1).

Transmission electron microscopy (TEM) analysis showed the formation of siderite nanorods (NRs) as the morphology of the iron nanoparticles with a different size depending on the reduction process (Fig. 2, Fig. S3†). The non-reduced hybrid contained $FeCO_3$ NRs with a size of approx. 7 nm in diameter × 59 nm in length (Fig. 2a), while the 15 min-reduced Fe-CALB hybrid contained $FeCO_3$ NRs of 5 nm in diameter × 40 nm in length (*the smallest reported as far as we know*) (Fig. 2b). Other reduced hybrids showed slightly longer nanorods with longer reduction times, which seems to indicate that the presence of the oxide species could be relevant in the growth of the nanorods (Fig. 2 and Fig. S4†).

Furthermore, the reduction step introduced magnetic properties to the hybrid, while the non-reduced hybrid did not show any magnetic capacity. Magnetism was also dependent on reduction time, and again the 15 min-reduced Fe-CALB hybrid exhibited an excellent magnetic response against a magnetic field, which allowed for rapid recovery. Analysis of the magnetic properties revealed a superparamagnetic material (zero remaining magnetization and coercivity) with a saturation magnetization value (M_s) of 125 emu g^{-1} (Fig. 3), extremely high compared to bulk siderite (M_s < 0.5 emu g^{-1}). These results could be explained considering the presence of a certain amount of amorphous Fe (0) in the hybrid generated by the reduction stage, which will be responsible for the magnetic behaviour.

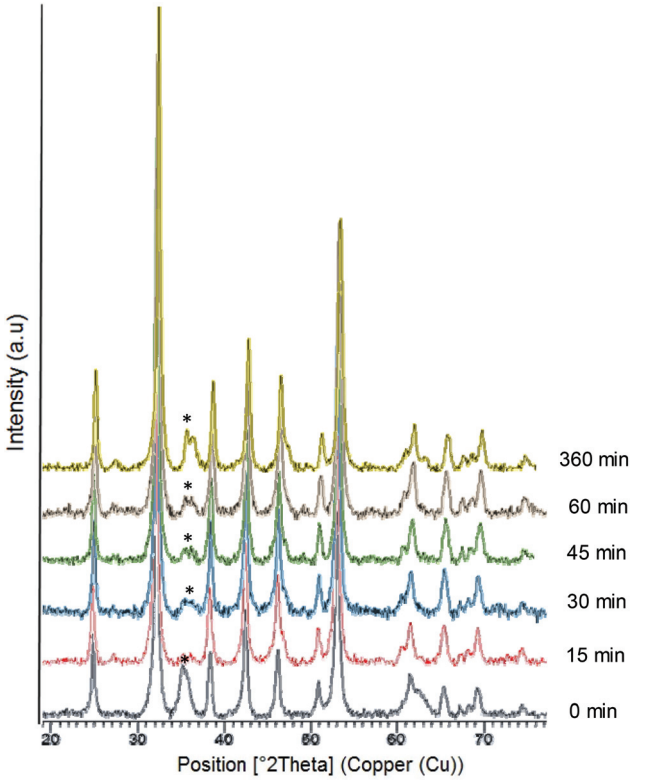

Fig. 1 X-Ray diffraction (XRD) patterns of the $FeCO_3$-CALB hybrid at different reducing times; (*) undesired oxide product.

These iron species could be, in principle, very sensitive to the oxidation, and therefore, a stabilization study was carried out. After one month left on the bench without any protection (no nitrogen atmosphere), the FeNR hybrid was characterized again. XRD and TEM analysis demonstrated the high stability of these iron species, and only a very slight increase of the peak at around 36° (iron oxide) was observed (Fig. S5†). This high stabilization can only be attributed to the presence of the enzyme. The enzyme induces the formation of this nanostructure by generating a protein network in which the iron nanoparticles are embedded. Therefore, the fact that the iron nanorods are around the superstructure of the enzyme aggregate protects them from oxidation. This seems to be a very interesting point, especially for iron that is extremely sensitive to oxidation conditions, and this is a key point for its application, for example, as a heterogeneous catalyst.

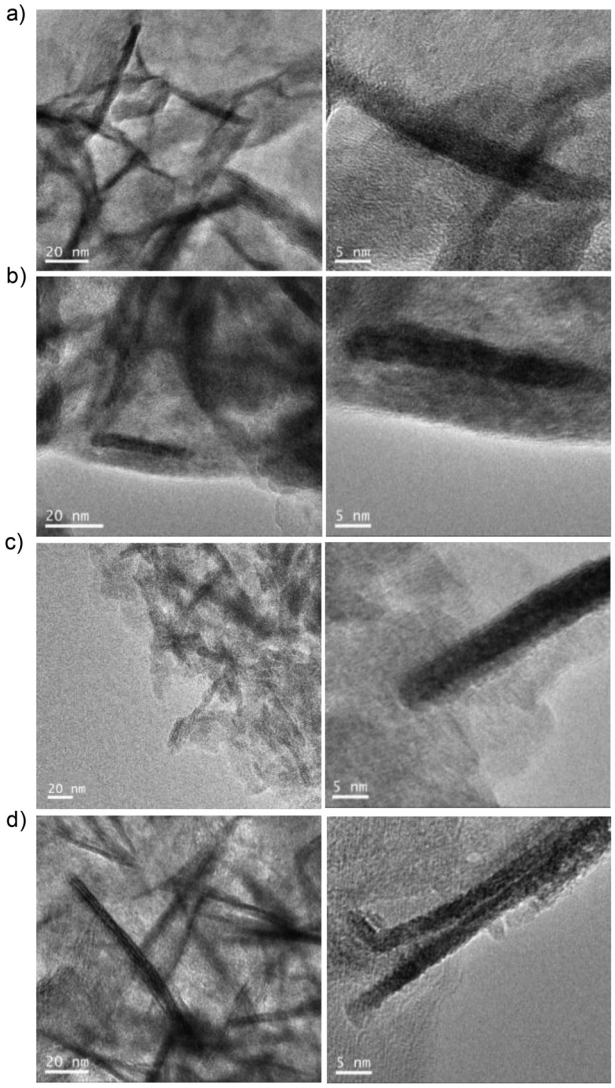

Fig. 2 TEM and HTEM images of different reduced-FeNRs-CALB hybrids: (a) non-reduced $FeCO_3$NRs-CALB, (b) 15 min-reduced $FeCO_3$NRs-CALB, (c) 30 min-reduced $FeCO_3$NRs-CALB, and (d) 45 min-reduced $FeCO_3$NRs-CALB or 60 min-reduced $FeCO_3$NRs-CALB.

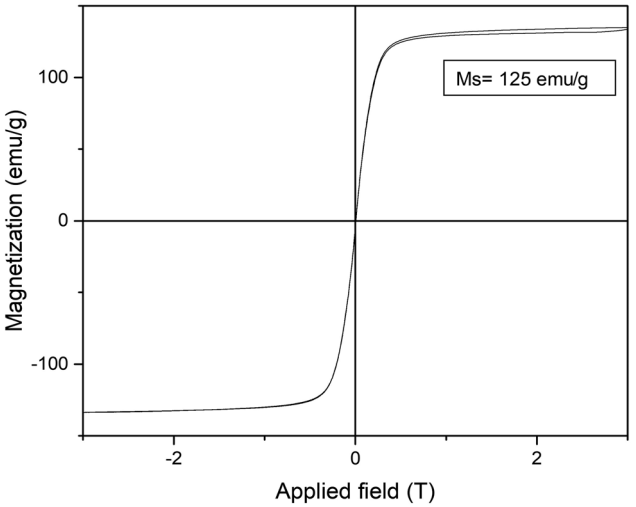

Fig. 3 Magnetization hysteresis loops of the 15 min-reduced Fe-CALB hybrid, normalized to the total mass of the sample (inset: saturation magnetization (M_s) value at 295 K).

At this point, this strategy allows multi-milligram amounts of a magnetic heterogeneous Fe hybrid material to be obtained. However, two different optimization processes were performed. The first one was to increase carbonate ions, by using 200 mM bicarbonate buffer instead of 100 mM. The second was to increase the amount of iron, using iron sulphate instead of the ammonium iron salt. The rest of the method was maintained (incubation time, agitation speed, reaction container, 15 min reduction, washing method). Previous tests showed that in these two cases, the pH of the mixture was adjusted to pH 8. A dark green/brown colour solid was obtained in both cases and XRD clearly demonstrated the formation of iron carbonate. The magnetic properties also showed the formation of a superparamagnetic material (data not shown). Other modifications, such as increasing the amount of reducing agent or changing the washing step by using magnetic means for separation instead of centrifugation, did not give significant differences in the protocol (data not shown).

Another approach tested was the reaction in distilled water without any buffer or additive. Two experiments were performed comparing the results with or without protein in the previous protocol with ammonium sulfate iron. Both solutions were incubated after 16 h as per the previous protocol, but no aggregate was formed. Then, we repeated the experiment and, after 30 min, the solution in both cases was reduced in the same way as previously described, immediately turning black. In both cases, a similar amount of solid (about 45 mg) was obtained, although less compared to the hybrids using the previous conditions (120 mg of FeNRs-CALB hybrids).

XRD analysis showed that in both cases, Fe (0) species were formed (Fig. 4); however, clear differences in structure were observed by TEM. The non-protein Fe(0) solid showed aggregate formation with very large Fe nanoparticles. However, using the enzyme, Fe nanoflowers (FeNFs) dispersed in the enzyme structure were generated (Fig. 4a and Fig. S6†). In the case of not using protein, a clear core of oxide could be observed in the TEM image, which did not occur in the protein–Fe(0)NFs (Fig. 4b and Fig. S7†). The analysis of the magnetic properties showed a saturation magnetization value (M_s) of 125–140 emu g^{-1} at 298 K (Fig. 4d), for both materials.

Therefore, this enzyme-induced strategy represents a simple way to produce stable superparamagnetic Fe(0) NFs.

Protein effect on the synthesis of Fe nanoparticles. Finally, the role of the protein structure in the final morphology and size of the iron nanoparticles was studied.

CALB is a lipase with a particular characteristic in the lipase family. It is one that has a very short oligopeptide lid, only four amino acids (critical for catalysis), and exists as a

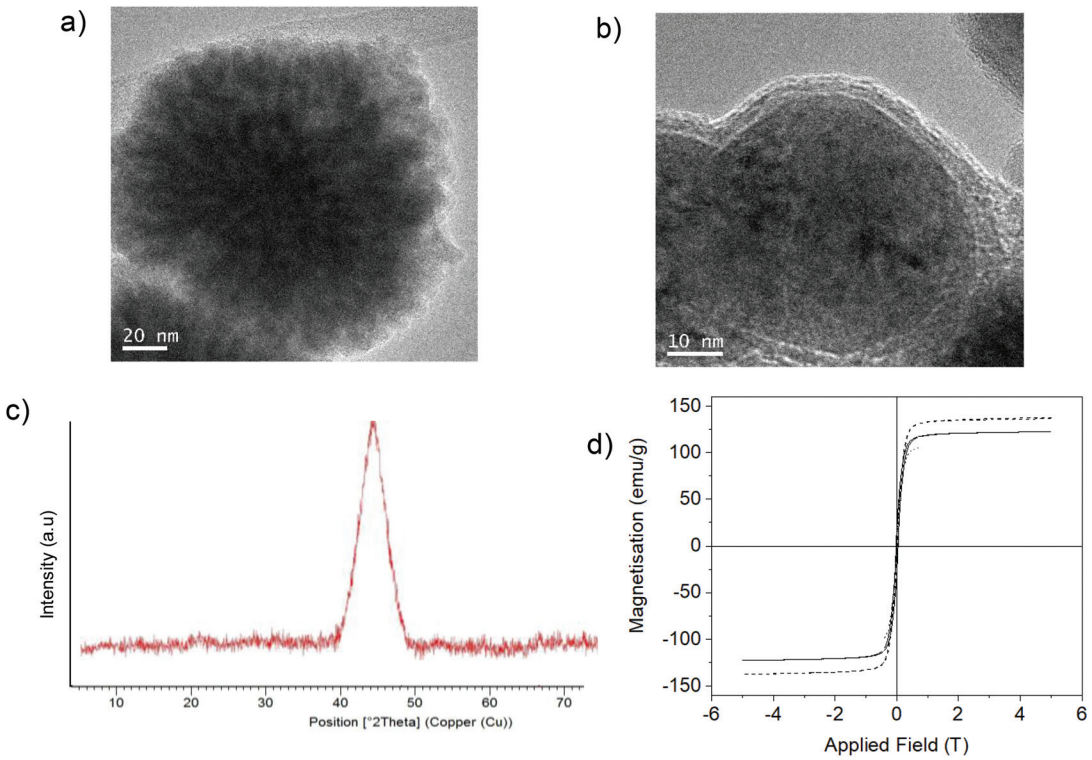

Fig. 4 Synthesis of Fe(0) hybrids. (a) A TEM image of Fe(0) nanoflowers of the material synthesized using CALB. (b) A TEM image of Fe(0) NPs of the material synthesized without using the enzyme. (c) The XRD pattern of Fe(0) in both cases. (d) Magnetization hysteresis loops of both Fe materials: FeNPs without protein (continuous line) and FeNFs-CALB (dashed line).

monomeric form in aqueous media (compared with most lipases that are in dimeric form).[22] In fact, CALB has a molecular weight of around 34 kDa, and many other lipases from different sources (for example, human monoacylglycerol, *Rhizomucor miehei*, *Pseudomonas fluorescens* or *Thermomyces lanuginosus* (TLL)) have a similar size,[22,23] although they have completely different behaviours.

Therefore, we first evaluated the effect of iron nanoparticles formation using TLL. In this case, two different approaches were performed using the commercial liquid enzyme directly (which is mainly in water as a dimer) and in the presence of Triton (monomeric TLL lipase in solution).

Using TLL dissolved in water, the reaction mixture with iron salt turned cloudy black after 45 min. Then, after reduction, a black solid was obtained, which clearly indicated the formation of different iron species to those obtained previously using CALB.

XRD analysis confirmed initial suspicions that the iron species was magnetite (Fe_3O_4) (matched well with JCPDS no. 79-0417) (Fig. 5a). TEM analysis showed that in this case different iron nanostructures (nanoflowers, nanorods, and nanosheets) were obtained (Fig. 5b). Surprisingly, using previously purified TLL solution, the iron species was magnetite (Fig. 5c), but the TEM analysis revealed a well-described homogeneous structure of nanorings (cyclic nanostructures) made up of well-organized iron nanoparticles (Fig. 5d). The purification of the enzyme led to the presence of detergent in the final enzyme solution,[24] which could be related to the final nanoring formation, although the presence of other contaminating enzymes in the commercial preparation of TLL could be the main reason for the formation of different nanostructures.[25]

Thus, direct hybrid preparation with lipase in a monomeric form, by adding detergent to the non-purified commercial preparation of TLL, was performed. In this case, a black solid was also provided (amount of multimilligrams), but the XRD analysis showed a different pattern, revealing in this case the formation of goethite (α-FeOOH) (matched well with JCPDS no. 17-0536) with a typical peak at 21° as the main species, but also containing magnetite (Fig. 5e). Also, TEM analyses revealed the formation of several morphologies (Fig. 5f).

For an explanation of how the protein can induce the formation of different iron species, three-dimensional enzyme structures were evaluated using bioinformatics tools. The key elements to consider are the particular amino acids that may be involved in metal coordination, such as Asp, Glu and His, and how they are distributed in the protein, such as the amino acid sequence and tertiary structure.

In particular, in the case of CALB, $FeCO_3$ was the main species generated, directly induced by the protein. In this case, direct formation of $FeCO_3$, where Fe(II) was stabilized by dative interactions with carboxylate side chains of glutamate or aspartate residues (binding sites) in CALB, as occurs in metalloproteins,[26] may be possible. Histidine residues are also a key group for iron coordination. The amino acid sequence and 3D

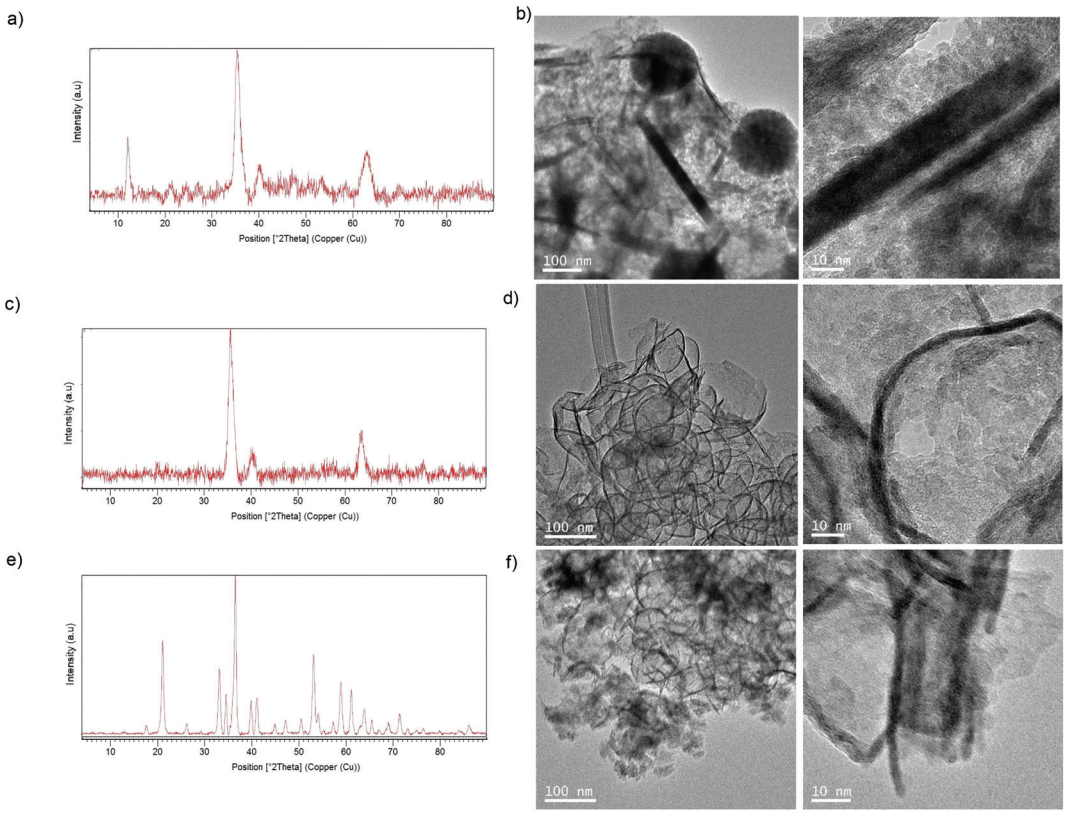

Fig. 5 Characterization of the synthesized TLL–Fe nanobiohybrids. (a) XRD pattern of Fe_3O_4 NPs using TLL. (b) TEM and HRTEM images of TLL–Fe_3O_4NPs. (c) XRD pattern of Fe_3O_4NPs using purified-TLL. (d) TEM and HRTEM images of TLL purified-Fe_3O_4NPs. (e) XRD pattern of the α-FeOOH/Fe_3O_4 TLL–Triton nanobiohybrid. (f) TEM and HRTEM images of the TLL–Triton–Fe nanobiohybrid.

protein structure of CALB (Fig. 6A, B and Fig. S8†) showed that this enzyme presents very few carboxylate residues, most of them as a single carboxylic acid residue without reactive histidine residues around (Fig. 6A). During hybrid formation and aggregation, a protein network is formed, so we can consider that iron(II) has a bidentate coordination with carboxylic groups on the protein, along with the bicarbonate molecule, conserving and stabilizing the structure of $FeCO_3$ as iron species (Fig. 6C). This is quite important because this iron species, as we have seen in the nanobiohybrid, is quite stable, preserving this structure for months. Therefore, the protein induces the formation and stabilization of the iron species, but also allows reproducibility of the methodology.

However, in TLL the situation is different. Analysing the structure of the protein and amino acids sequence (Fig. 7 and Fig. S9†), we can see that this enzyme has 31 carboxylate groups, mainly all on the surface, and four reactive histidine residues, two of them particularly on the surface (His109 and His134) (Fig. 7A).

This phenomenon is clearly quite important for the final formation of iron species. The amount of carboxylic groups and the fact that many of them are on at least two sufficiently close residues have great influence on the coordination of iron, displacing the carbonate and allowing more water molecules to be introduced in the coordination (Fig. 7B). Furthermore, His also has a great influence, because some of the iron atoms can coordinate with the imidazole residue of His, making the formation of Fe(III) species more accessible. This situation could explain the formation of magnetite as the only iron species. This also seems to indicate that this coordination causes the formation of iron oxides species.

However, the iron species generated by TLL in the presence of polyethylene glycol *tert*-octylphenyl ether (Triton X-100) at a relative high concentration (0.5% w/v) was mainly goethite (α-FeOOH), containing also magnetite as an iron species. Triton X-100 molecules present a hydrophobic part that has a tendency to interact by aromatic stacking interactions or simple hydrophobic interactions with hydrophobic residues in the enzyme. Analysing the 3D-structure of the protein, emphasizing the hydrophobic groups (Fig. S10†), we can observe that carboxylates and imidazole residues are right next to the hydrophobic ones in many cases. Thus, we postulate that this interaction could affect the entire coordination system between the iron atoms and protein residues, which could allow the incorporation of oxygen molecules, facilitating the oxidation of almost all Fe(II) atoms to Fe(III) to finally form oxo-hydroxy species (Fig. S10†). Also in these nanobiohybrids, the magnetic properties were different at room temperature (Fig. 8). The hybrid has a magnetization saturation value (M_s) of 60 emu g^{-1} using exclusively TLL or purified TLL, lower

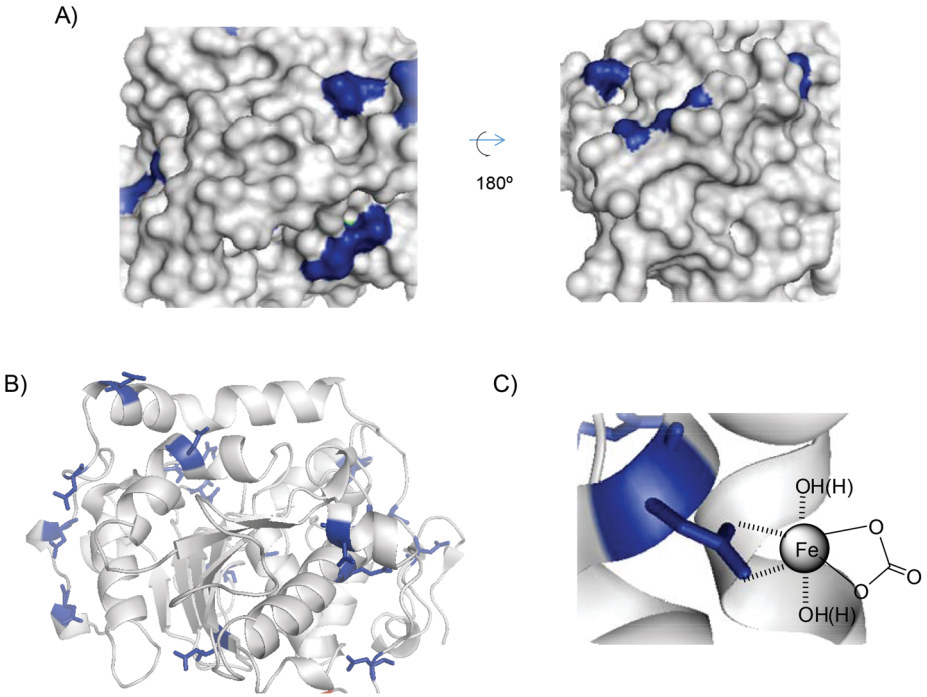

Fig. 6 (A) 3D-surface of CALB with Asp and Glu residues highlighted in blue. (B) 3D-structure of CALB. (C) $FeCO_3$–protein coordination complex. Figures were prepared using the Pymol program using PDB file 1TCA.

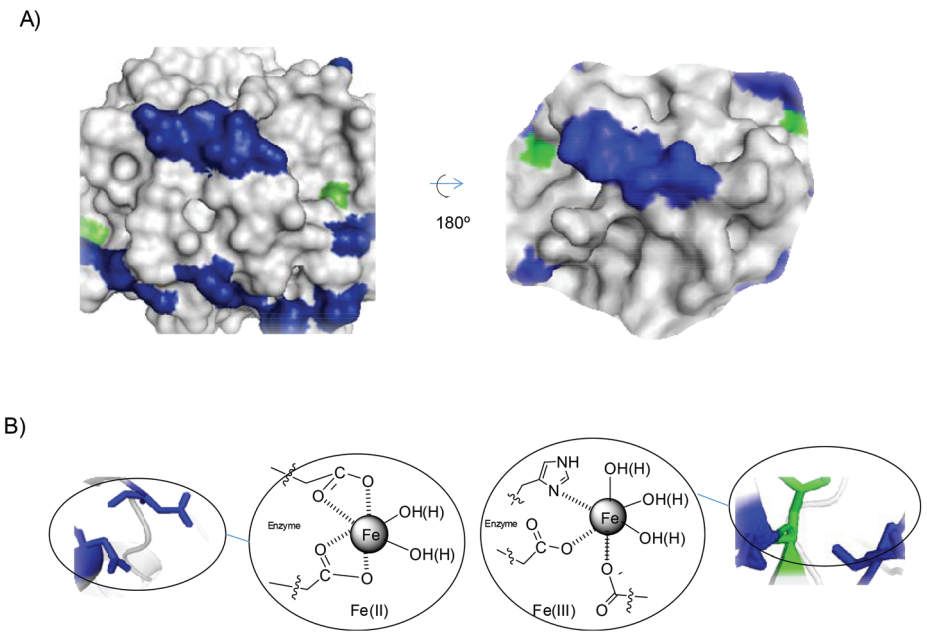

Fig. 7 (A) 3D-surface of TLL with several amino acid residues marked: Asp and Glu residues (blue), and His (green). (B) Proposed iron coordination species induced by the protein. The Pymol program using PDB file 1DT3 was used to prepare figures.

than that of bulk magnetite (92 emu g^{-1}). However, a M_s value of 10 emu g^{-1} was measured for the hybrid prepared in the presence of detergent, due to the magnetite content in the material, with goethite being the main species with an antiferromagnetic behaviour.

After these interesting results, larger proteins were used (Fig. 9). In this case, another lipase from *Candida rugosa* (CRL) (63 kDa as a monomer) and tyrosinase from mushroom (*Agaricus* bisporus) (TYR) (122 kDa as a tetramer) were used. In all cases, the enzymes without additives showed molecular

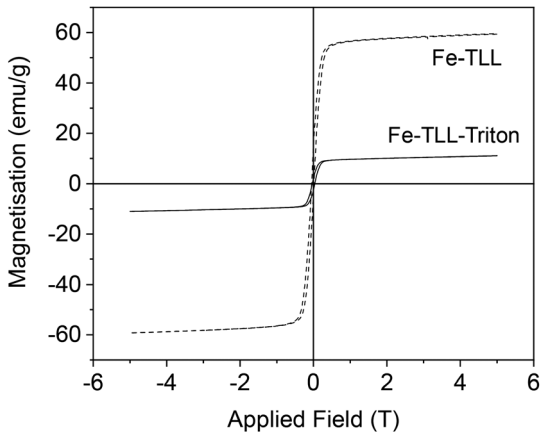

Fig. 8 Magnetization hysteresis loops of both Fe–TLL materials.

weight >100 kDa, which is three times more than the enzymes previously tested. 65 mg of a brown-red solid was obtained using CRL, whereas 30 mg of a brown solid was obtained using TYR. XRD showed an amorphous structure for CRL, while a goethite pattern (matched well with JCPDS no. 17-0536) was obtained using TYR. TEM analyses revealed the formation of longer nanosheets for CRL (50–>100 nm) (Fig. 9a) and shorter nanosheets (around 30–40 nm) for TYR (Fig. 9c). Spheroidal nanoparticles were obtained with CRL when Triton was used as an additive (Fig. 9b).

The magnetic properties of the hybrids depend on the iron species that has been formed. The Fe hybrid synthesized using tyrosinase showed a similar ferromagnetic behaviour with a M_s value similar to that obtained with TLL + Triton (10 emu g^{-1}) (Fig. 8), while the hybrid materials obtained from CRL showed a paramagnetic behaviour with M_s values in both cases of 1.5 emu g^{-1}, which seems to indicate the possible formation of hematite (Fig. 9d–f).

Evaluating the amino acid sequence and 3D structure of both enzymes, we could find that in the case of CRL (Fig. S11 and S12†), a large hydrophobic pocket can be observed. In this case, as well as in the artificial hydrophobic interactions between TLL and detergent, the protein can modulate the coordination of the iron on the protein surface. Forty-eight carboxylate groups and four His residues are found in CRL, which, like TLL, can induce the formation of iron oxides instead of carbonate, but in this case the main species appears to be hematite, where complete oxidation was possible due to internal hydrophobic group interactions.

In the case of tyrosinase, the largest protein used here, we can observe the presence of seventy-seven Asp/Glu residues and twenty-two His residues in each dimer in the amino acid sequence (Fig. S13†), considering this protein as a homodimer (Fig. S14†). Evaluating the 3D-surface on the entire protein, we can observe a large number of iron binding groups on the surface, but also hydrophobic residues in the near environment (Fig. S14†). As we observed in the case of using detergent, tyrosinase is able to coordinate iron, forming iron oxide as magnetite without additive, but it produces the oxohydroxy iron species as the main one in the material.

Other tested proteins such as ovalbumin or catalase produced extremely low amounts of hybrids with different magnetic properties (Fig. S15†).

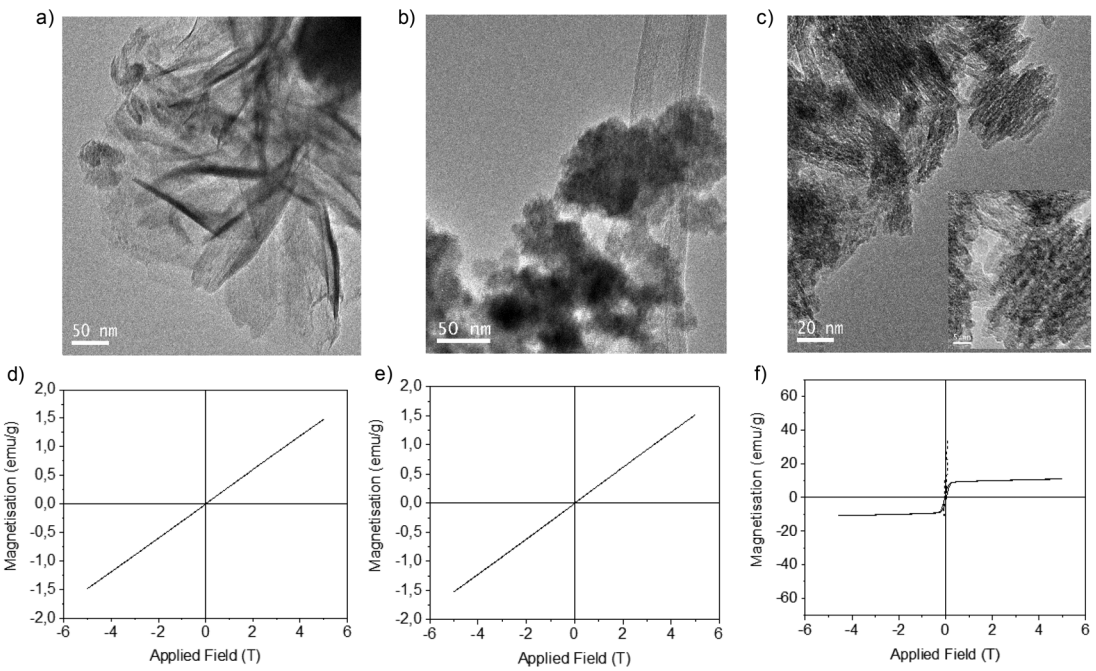

Fig. 9 Characterization of different Fe–enzyme nanohybrids. (a–c) TEM images of Fe hybrids synthesised using different enzymes (CRL (a), CRL with Triton (b), and TYR (c)). (d and e) Magnetization hysteresis loops (CRL (d), CRL with Triton (e), and TYR (f)).

Application of Fe nanoparticles-enzyme hybrids in heterogeneous catalysis

Chemoselective hydrogenation of arenes. The catalytic efficiency of the different Fe nanoparticles-enzyme hybrids was tested in the chemoselective hydrogenation of *p*-nitrophenol (*p*NP) to *p*-aminophenol (*p*AP) (Table 1). The reaction was carried out in aqueous media and at room temperature. Different enzyme solutions were tested in the reaction and no activity was found in any case (data not shown).

The superparamagnetic hybrids 15 min-reduced $FeCO_3$NRs-CALB and Fe(0)NFs-CALB showed the best performance, with a complete reduction in 30 seconds (Table 1, entries 2 and 7). In the case of siderite hybrids, the efficiency can be related to the length of the nanorods and also to the presence of oxide species, with the non-reduced being the worst, inactive in the reaction (Table 1, entry 1). In the case of the Fe (0) nanostructure hybrid, it was clear that Fe(0)NFs-CALB was much more efficient (10-fold) than FeNPs synthesized without protein (Table 1, entries 7 and 8).

For the other Fe nanobiohybrids, it was clear that the magnetite hybrids were catalytically slower than the others, by four times compared with the best, but much more efficient than the goethite nanobiohybrid, especially using tyrosinase as protein, where only 50% conversion was found after 10 min. Using CRL, no active catalyst was obtained (Table 1, entries 12 and 13).

All heterogeneous catalysts were easily recovered after the reaction. In particular, the most active in the reaction, 15 min-reduced $FeCO_3$NRs-CALB and Fe(0)NFs-CALB, were reused after six reaction cycles, retaining more than 95% of their catalytic efficiency thereafter.

C–C bonding reactions. Taking into account the excellent results in the hydrogenation reaction, the catalytic performance of the 15 min-reduced $FeCO_3$NRs-CALB hybrid was tested in the Heck-reaction between iodobenzene (IB) and ethyl acrylate (EA) under different conditions (Table 2) without any iron initiator. This is a typical reaction well described especially for Pd catalysis, but only a few examples using iron catalysis have been reported.[27,28]

Initially, the reaction was performed in DMF and DMF (dry) at 65 °C using triethylamine as base (Table 2, entries 1 and 2). Unfortunately, a trace amount of the desired product was

Table 1 Hydrogenation of *p*-nitrophenol catalysed by FeNP-enzyme hybrids[a]

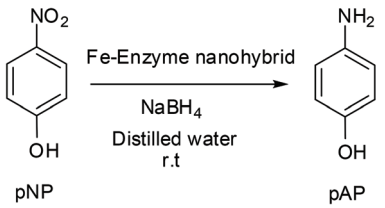

Entry	Catalyst	Time (min)	Yield of *p*AP (%)
1	Non-reduced $FeCO_3$NRs-CALB	20	0
2	15 min-reduced $FeCO_3$NRs-CALB	0.5[b]	>99[b]
3	30 min-reduced $FeCO_3$NRs-CALB	1	>99
4	45 min-reduced $FeCO_3$NRs-CALB	1.5	>99
5	60 min-reduced $FeCO_3$NRs-CALB	1.5	>99
6	360 min-reduced $FeCO_3$NRs-CALB	4	92
7	Fe(0)NFs-CALB	0.5	>99
8	Fe(0)NPs	5	>99
9	Fe_3O_4NPs-TLL	2	>99
10	Fe_3O_4NPs-purified-TLL	2	>99
11	FeOOH/Fe_3O_4–TLL(+Triton)	8	>99
12	Fe_2O_3-CRL	20	0
13	Fe_2O_3-CRL(+Triton)	20	0
14	FeOOH/Fe_3O_4-Tyr	10	50

[a] Conditions: 1.0 mM (3 mg) *p*NP, 40 mM (3 mg) $NaBH_4$, 2 mL of distilled water, 3 mg of Fe-catalyst, air and room temperature. [b] The same results were found with the hybrid prepared using $FeSO_4$ or the optimized protocol using 200 mM bicarbonate in the synthesis.

Table 2 Heck coupling of iodobenzene and ethyl acrylate catalysed by the 15 min-reduced $FeCO_3$NRs-CALB hybrid

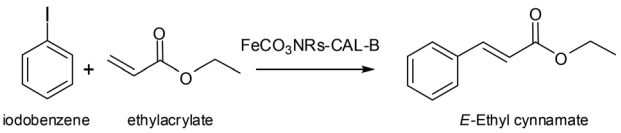

iodobenzene ethylacrylate *E*-Ethyl cynnamate

Entry	Solvent	Additive	*T* (°C)	Base	Time (h)	Yield of ethyl cinnamate[b] (%)
1	DMF	—	65	NEt_3	24	Trace[a]
2	DMF (dry)	—	65	NEt_3	24	Trace[a]
3	DMF (dry)	—	90	NEt_3	24	Trace[a]
4	DMF (dry)	—	90	Na_2CO_3	24	2.2[a]
5	DMF (dry)	—	90	^{t}BuOOK	24	Trace[a]
6	DMF (dry)	—	90	DIPEA	24	Trace[a]
7	DMF (dry)	DMAP	90	^{t}BuOOK	24	Trace[c]
8	DMF (dry)	Molecular sieves 3 Å[e]	90	NEt_3	24	20[a]
9	DMF (dry)	Molecular sieves 3 Å[e]	90	NEt_3	72	56[a]
10	DMF (dry)	Molecular sieves 3 Å[e]	90	Na_2CO_3	24	<1[a,d]

[a] Conditions: Iodobenzene (0.0274 mmol), ethyl acrylate (0.055 mmol), 1 mL of solvent, 2 equiv. base, 5 mg of catalyst. [b] Yield of product was determined by crude product. [c] Conditions: Iodobenzene (0.091 mmol), ethyl acrylate (0.45 mmol), 1 mL of solvent, 4 equiv. base, 5 equiv. DMAP, 5 mg of catalyst. [d] Mainly produced *cis*-ethyl cinnamate (total conversion: 3%). [e] 18 mg.

Table 3 Degradation of Bisphenol A (BPA) catalysed by Fe-CALB hybrids[a]

Entry	Catalyst	H_2O_2 [mM]	Degradation yield of BPA (%)
1	Non-reduced $FeCO_3$NRs-CALB	50	50
2	Non-reduced $FeCO_3$NRs-CALB	100	68
3	15 min-reduced $FeCO_3$NRs-CALB	50	55
4	15 min-reduced $FeCO_3$NRs-CALB	100	70
5	15 min-reduced $FeCO_3$NRs-CALB-200 mM	100	90

[a] 0.2 mM BPA, 2 ml of sodium acetate buffer 100 mM pH 4, 3 mg of catalyst, 20 h, r.t.

found. Then, the reaction temperature was increased to 90 °C, but no change was observed (entry 3). Therefore, different bases were tested and only slight conversion was observed with sodium carbonate (entry 4). Even the use of *tert*-butoxide, which was described as an adequate base for iron catalysis, did not work, even in the presence of DMAP (entry 7).

Considering the possibility of some water in the solution as a problem, molecular sieves were added in an upcoming reaction. Using triethylamine as base, 20% yield of *E*-ethyl cinnamate was produced in 24 h and a 56% yield was achieved after 72 h incubation (entries 8 and 9). The reaction was also tested with sodium carbonate and molecular sieves, but a yield of less than 1% was achieved after 24 h (entry 10).

Environmental degradation of organic pollutants

An important application of cheap and effective catalysts is the removal of toxic organic molecules from water. Here, we demonstrated the catalytic effectiveness of this 15 min-reduced $FeCO_3$NRs-CALB hybrid in the degradation of Bisphenol A (BPA) (an important molecule in the chemical industry, but highly toxic).

Different $FeCO_3$NRs hybrids were tested in the degradation of BPA (Table 3). Initial experiments evaluated the reaction at different pHs. Finally, the best conditions were determined as acidic pH (acetate buffer pH 4) and two different concentrations of H_2O_2 were tested as an oxidant (Table 3). CALB solution was firstly tested in the reaction and no conversion was found (data not shown). Under these conditions, the catalyst prepared using 200 mM bicarbonate (15 min-reduced $FeCO_3$NRs-CALB-200 mM) showed the best result, degrading 90% of BPA in 20 h using 100 mM of hydrogen peroxide as oxidant, an improvement over the results achieved with the 15 min-reduced $FeCO_3$NRs-CALB (70%). In this case, the non-reduced $FeCO_3$NRs-CALB also showed good yields in the Fenton reaction (Table 3). The addition of less amount of H_2O_2 (50 mM) resulted in lower degraded yields.

Conclusions

A strategy has been developed to synthesize iron nanoparticles-enzyme hybrids with good control of the iron species and nanoparticle morphology. Enzymes directly induce the formation of different inorganic iron species, from superparamagnetic $FeCO_3$/Fe(0) nanorods or Fe(0) nanoflowers, to Fe_3O_4 nanosheets, nanoflowers, nanorings or goethite or hematite nanosheets. The Fe nanoparticles-enzyme nanobiohybrid consists of a material composed of iron nanoparticles homogeneously distributed in a protein matrix that confers massive stability against aggregation and oxidation, which is critical for catalysis and for metal iron nanoparticles.

It has been shown that the structure of the enzyme, considering its rear arrangement as well as its amino acid structure, leads to specific interactions with iron ions that determine the formation of one species or another. Therefore, the initial Fe complexes are responsible for the final iron species.

Furthermore, optimization of the synthesis method allows the preparation of highly magnetically charged hybrids, despite the presence of the protein matrix. These hybrids have a very high magnetic response, preserving their superparamagnetic behaviour. This unique property exhibited by nanoscale magnetic materials, along with multiple chemical surface possibilities, offers exciting new opportunities in different areas.

Here we have demonstrated the great capacity of the hybrids as heterogeneous catalysts in different processes, such as the chemoselective hydrogenation of arenes, C–C bonding reactions, and organic pollutant elimination processes. The ability to control the species and shape of nanoparticles, as well as their magnetism, makes these enzyme-induced processes very promising for the future design and application of nanomaterials in different areas.

Experimental

General

Candida antarctica B lipase (Lipozyme® CALB) (CALB) and *Thermomyces lanuginosus* lipase (TLL) solution (Lipozyme® TL 100L) were from Novozymes (Denmark). Ammonium iron(II) sulphate hexahydrate [$(NH_4)_2Fe(SO)_2 \times 6H_2O$ (Mohr's salt)], hydrogen peroxide (33%), iron sulphate, *Candida rugosa* lipase powder (TypeVII) (CRL), tyrosinase from mushrooms (TYR), iodobenzene, DMF, *p*-nitrophenol, *p*-nitroamino, ethyl acrylate, Bisphenol A, sodium bicarbonate and sodium borohydride were purchased from Sigma-Aldrich. HPLC grade acetonitrile was purchased from Scharlab.

Inductively coupled plasma atomic emission spectrometry (ICP-AES) was performed on PerkinElmer OPTIMA 2100 DV equipment. The X-Ray diffraction (XRD) pattern was obtained using a Texture Analysis Diffractometer D8 Advance (Bruker) with Cu Kα radiation. The transmission electron microscopy (TEM) and high resolution TEM microscopy (HRTEM) analyses were performed on a JEOL 2100F microscope equipped with an INCA x-sight EDX detector (Oxford Instruments). To recover the biohybrids, a Biocen 22 R (Orto-Alresa, Spain) refrigerated centrifuge was used. The spectrophotometric analyses were run on a V-730 spectrophotometer (JASCO, Japan). HPLC spectrum P100 (Thermo Separation products) was used. Analyses

were run at 25 °C using an L-7300 column oven and a UV6000LP detector.

The magnetic characterization of the samples was recorded in a vibrating sample magnetometer (MLVSM9, MagLab 9T, VSM, Oxford Instrument). The samples were accurately weighed and fitted into gelatine capsules for magnetic measurements. Hysteresis loops of the powdered samples were measured at room temperature applying a magnetic field of ±3T.

General synthesis of the Fe nanoparticles-enzyme hybrids

A corresponding amount of enzyme was added to 60 mL of sodium bicarbonate buffer 0.1 M (or 0.2 M) pH = 10 in order to finally achieved an enzyme concentration of 0.27–0.3 mg ml^{-1}. In the case of CALB solution, 1.8 ml (9 mg lipase per mL determined by Bradford assay) was added. 0.75 mL of TLL solution (24 mg ml^{-1} determined by Bradford assay), 0.5 g of CRL powder and 15 mg of commercial extract Tyr, were used respectively. The corresponding enzyme solution was poured into a 100 mL glass bottle containing a small magnetic bar stirrer (12 × 4.5 mm). The solution was stirred in a magnetic agitator at 380 rpm (*this is an important point for avoiding iron oxidation*) for 1–2 min. In some cases, 0.25% (w/v) Triton X-100 was added to the enzyme solution. Then, 600 mg of Fe $(NH_4)_2(SO_4)_2{\cdot}6H_2O$ (or $FeSO_4$) (10 mg ml^{-1}) was added to the protein solution and it was maintained for 16 hours at room temperature stirring at 380 rpm After the first 30 min incubation, the solution turned cloudy (greenish gray) and the pH solution was measured indicating a decrease from 10 to 8. After 16 h incubation, the solid was recovered and re-suspended in 15 mL of water or treated with $NaBH_4$ (300 mg dissolved in 6 mL of water added in two lots of 3 mL) incubated at different times (15, 30, 60, 90 and 360 min) and then recovered and re-suspended in 15 mL of water. Then, in all cases, the solid was washed with distilled water (15 mL × 3). In the case of previous use of borohydride, the pH of the final washing water must be around 5 to avoid residues of sodium borohydride and its interaction with the freeze-drying. Finally, the supernatant was removed and the pellet of each falcon was re-suspended in 2 mL of water, collected in a cryotube, frozen with liquid nitrogen and lyophilized for 16 hours. Characterization of the different nanobiohybrids was performed by XRD and TEM analysis.

Catalytic reduction of 4-nitrophenol (*p*NP) to 4-aminophenol (*p*AP)

p-Nitrophenol (*p*NP) was dissolved in 2 mL of distilled water at 1 mM concentration. Then, solid $NaBH_4$ (3.2 mg) was added to the solution. After this addition, the light yellow solution changes to a strong yellow colour, generating the formation of 4-nitrophenolate ions (substrate UV-peak undergoes an immediate shift from 317 to 400 nm). After 30 seconds, 3 mg of the different Fe hybrids were added under gentle stirring at room temperature in an orbital shaker. The reaction progress was monitored by taking out an aliquot of the solution (0.1 mL) at different times, diluting it with distilled water (2 mL) and measuring the absorption spectrum between 500 and 300 nm in a quartz cuvette.

General procedure for the Heck reaction

Iodobenzene (0.0306 mL, 0.274 mmol) and ethyl acrylate (0.059 mL, 0.55 mmol) were dissolved in 1 mL of DMF or dry DMF in a 20 mL screw-sealed vessel. Then, 5 mg of 15 min-reduced $FeCO_3$NRs-CALB nanobiohybrid (14.9 mol%) was added. After 5 min of preheating at the corresponding T (65 °C or 90 °C), 2 equiv. of base was added to initialize the reaction. The final suspension was left under vigorous magnetic stirring for the indicated times. The reaction progress was monitored by HPLC analysis of samples withdrawn at different times. The analysis was performed with a Kromasil-C8 column (150 × 4.6 mm and 5 μm Ø), at a flow of 1.0 mL min^{-1}; λ: 250 nm and mobile phase: 50% (v/v) ACN in MilliQ water. In these conditions, the retention times were: 4.27 min for ethyl acrylate, 11.32 min for (*E*)-ethyl cinnamate and 13.66 min for iodobenzene. The stereochemistry was confirmed by HPLC using the (*E*) and (*Z*)-ethyl acrylate standards (*Z* had a retention time of 10.38 min). The yields were obtained by extrapolating the values through a calibration curve of the product (R^2 = 0.9964).

Catalytic degradation of Bisphenol-A (BPA)

A solution of BPA in acetonitrile (10 mM) was prepared. 0.2 ml of this solution was dissolved in 10 mL of 100 mM sodium acetate buffer pH 4 up to a 0.2 mM concentration of BPA. Hydrogen peroxide (33% in water v/v) was added to this BPA solution to achieve different concentrations (50 or 100 mM). To initialize the reaction, 3 mg of catalyst was added to 2 mL of BPA solution and the reaction was maintained under gentle stirring at room temperature in an orbital shaker (320 rpm). Samples (50 μl) at different times were taken, to follow the reaction, and analysed by RP-HPLC. The samples were diluted 5 times in a mixture of distilled water/acetonitrile (1/1) before injection. The HPLC column was a C8 Kromasil 150 × 4.6 mm AV-2059. The HPLC conditions used were: an isocratic mixture of 50% acetonitrile and 50% ultrapure water, UV detection at 225 nm using a Diode array detector, and a flow rate of 1 mL min^{-1}. Under these conditions, the retention times of the substrates were 1.57 min for H_2O_2 and 4.90 min for BPA.

Conflicts of interest

There are no conflicts to declare.

Acknowledgements

The authors acknowledge support from the Spanish National Research Council (CSIC) (CSIC-PIE 201880E011). This research was supported by SAMSUNG L.S (GRO PROGRAM 2017). We also thank the Ministry of Education, Youth and Sports of the Community of Madrid and the European Social Fund for a contract to C. P.-R. (PEJD-2017PRE/SAL-3762) in the program

of Youth Employment and the Youth Employment Initiative (YEI) 2017. We also thank Ramiro Martínez from Novozymes.

References

1 A. G. Roca, L. Gutiérrez, H. Gavilán, M. E. Fortes Brollo, S. Veintemillas-Verdaguer and M. P. Morales, Design strategies for shape-controlled magnetic iron oxide nanoparticles, *Adv. Drug Delivery Rev.*, 2019, **38**, 68–104.
2 Y. Xiao and J. Du, Superparamagnetic nanoparticles for biomedical applications, *J. Mater. Chem. B*, 2020, **8**, 354–367.
3 M. Neamtu, C. Nadejde, V.-D. Hodoroaba, R. J. Schneider, L. Verestiuc and U. Panne, Functionalized magnetic nanoparticles: Synthesis, characterization, catalytic application and assessment of toxicity, *Sci. Rep.*, 2018, **8**, 6278.
4 C. Kuppe, K. R. Rusimova, L. Ohnoutek, D. Slavov and V. K. Valev, "Hot" in Plasmonics: Temperature-Related Concepts and Applications of Metal Nanostructures, *Adv. Opt. Mater.*, 2019, **8**, 1901166.
5 T. Hiemstra, Surface structure controlling nanoparticle behavior: magnetism of ferrihydrite, magnetite, and maghemite, *Environ. Sci.: Nano*, 2018, **5**, 752–764.
6 S. Behrens and I. Appel, Magnetic nanocomposites, *Curr. Opin. Biotechnol.*, 2016, **39**, 89–96.
7 I. Bauer and H.-J. Knölker, Iron Catalysis in Organic Synthesis, *Chem. Rev.*, 2015, **115**, 3170–3387.
8 A. Fürstner, Iron Catalysis in Organic Synthesis: A Critical Assessment of What It Takes To Make This Base Metal a Multitasking Champion, *ACS Cent. Sci.*, 2016, **2**, 778–789.
9 Q. Liang and D. Song, Iron N-heterocyclic carbene complexes in homogeneous catalysis, *Chem. Soc. Rev.*, 2020, **49**, 1209–1232.
10 S. Shylesh, V. Schnemann and W. R. Thiel, Magnetically separable nanocatalysts: bridges between homogeneous and heterogeneous catalysis, *Angew. Chem., Int. Ed.*, 2010, **49**, 342–359.
11 F. N. Sayed and V. Polshettiwar, Facile and Sustainable Synthesis of Shaped Iron Oxide Nanoparticles: Effect of Iron Precursor Salts on the Shapes of Iron Oxides, *Sci. Rep.*, 2015, **5**, 9733.
12 X. Xie, Y. Li, Z. Q. Liu, M. Haruta and W. Shen, Low-temperature oxidation of CO catalysed by Co(3)O(4) nanorods, *Nature*, 2009, **458**, 746–749.
13 S. Behrens and I. Appel, Magnetic nanocomposites, *Curr. Opin. Biotechnol.*, 2016, **39**, 89–96.
14 K. An and G. A. Somorjai, Size and Shape Control of Metal Nanoparticles for Reaction Selectivity in Catalysis, *ChemCatChem*, 2012, **4**, 1512–1524.
15 M. Kumar, H. S. Dosanjh, Sonika, J. Singh, K. Monira and H. Singh, Review on magnetic nanoferrites and their composites as alternatives in waste water treatment: synthesis, modifications and applications, *Environ. Sci.: Water Res. Technol.*, 2020, **6**, 491–514.
16 W. Ling, M. Wang, C. Xiong and D. Xie, Synthesis, surface modification, and applications of magnetic iron oxide nanoparticles, *J. Mater. Res.*, 2019, **34**, 1828–1844.
17 D. Lopez-Tejedor, R. Benavente and J. M. Palomo, Iron Nanostructured catalysts: Design and applications, *Catal. Sci. Technol.*, 2018, **8**, 1754–1776.
18 F. Hof, M. Liu, G. Valenti, E. Picheau, F. Paolucci and A. Pénicaud, Size Control of Nanographene Supported Iron Oxide Nanoparticles Enhances Their Electrocatalytic Performance for the Oxygen Reduction and Oxygen Evolution Reactions, *J. Phys. Chem. C*, 2019, **123**, 20774–20780.
19 A. Mansouri and N. Semagin, Palladium islands on iron oxide nanoparticles for hydrodesulfurization catalysis, *Catal. Sci. Technol.*, 2018, **8**, 2323–2332.
20 R. Benavente, D. Lopez-Tejedor and J. M. Palomo, Synthesis of a superparamagnetic ultrathin FeCO3 nanorods–enzyme bionanohybrid as a novel heterogeneous catalyst, *Chem. Commun.*, 2018, **54**, 6256–6259.
21 M. Filice, M. Marciello, M. P. Morales and J. M. Palomo, Synthesis of heterogeneous enzyme–metal nanoparticle biohybrids in aqueous media and their applications in C–C bond formation and tandem catalysis, *Chem. Commun.*, 2013, **49**, 6876–6878.
22 J. M. Palomo, M. Fuentes, G. Fernández-Lorente, C. Mateo, J. M. Guisan and R. Fernández-Lafuente, General Trend of Lipase to Self-Assemble Giving Bimolecular Aggregates Greatly Modifies the Enzyme Functionality, *Biomacromolecules*, 2003, **4**(1), 1–6.
23 T. P. Dinh, D. Carpenter, F. M. Leslie, T. F. Freund, I. Katona, S. L. Sensi, S. Kathuria and D. Piomelli, Brain monoglyceride lipase participating in endocannabinoid inactivation, *Proc. Natl. Acad. Sci. U. S. A.*, 2002, **99**, 10819–10824.
24 J. M. Palomo, M. Filice, R. Fernandez-Lafuente, M. Terreni and J. M. Guisan, Regioselective Hydrolysis of Different Peracetylated b-Monosaccharides by Immobilized Lipases from Different Sources. Key Role of The Immobilization, *Adv. Synth. Catal.*, 2007, **349**, 1969–1976.
25 V. G. Tacias-Pascacio, S. Peirce, B. Torrestiana-Sánchez, M. Yates, A. Rosales-Quintero, J. J. Virgen-Ortíz and R. Fernandez-Lafuente, Evaluation of different commercial hydrophobic supports for the immobilization of lipases: Tuning their stability, activity and specificity, *RSC Adv.*, 2016, **6**, 100281–100294.
26 S. Barber-Zucker, B. Shaanan and R. Zarivach, Transition metal binding selectivity in proteins and its correlation with the phylogenomic classification of the cation diffusion facilitator protein family, *Sci. Rep.*, 2017, **7**, 16381.
27 K. Zhu, J. Dunne, M. P. Shaver and S. P. Thomas, Iron-catalyzed heck-type alkenylation of functionalized alkyl bromides, *ACS Catal.*, 2017, **7**, 2353–2356.
28 R. Loska, C. M. R. Volla and P. Vogel, Iron-catalyzed Mizoroki-Heck Cross-Couplin Reaction with styrenes, *Adv. Synth. Catal.*, 2008, **350**, 2859–2864.